InSAR measured permafrost degradation of palsa peatlands in northern Sweden

Authors: Samuel Valman[1,2]*, Matthias B. Siewert[3]*, Doreen Boyd[2], Martha Ledger[4,5], David Gee[6], Betsabe de la Barreda-Bautista[4,2], Andrew Sowter[6], Sofie Sjogersten[4]

Affiliations:

[1] Nottingham Geospatial Institute, University of Nottingham, Nottingham NG7 2TU, UK

[2] School of Geography, University of Nottingham, University Park, NG7 2RD, Nottingham, UK

[3] Department of Ecology and Environmental Sciences, Umeå University, Umeå, Sweden

[4] School of Biosciences, University of Nottingham, Sutton Bonington Campus, College Road, LE12 5RD, Loughborough, UK

[5] School of Biological Sciences, Kadoorie Biological Sciences Building, University of Hong Kong, Pok Fu Lam Road, Hong Kong

[6] TerraMotion, Ingenuity Centre, Triumph Rd, Nottingham NG7 2TU

*These authors contributed equally to this work.

Corresponding author: Sofie Sjögersten sofie.sjogersten@nottingham.ac.uk

Abstract. Climate warming is degrading palsa peatlands across the circumpolar permafrost region. Permafrost degradation may lead to ecosystem collapse and potentially strong climate feedbacks, as this ecosystem is an important carbon store and can transition to being a strong greenhouse gas emitter. Landscape level measurement of permafrost degradation is needed to monitor this impact of warming. Surface subsidence is a useful metric of change in palsa degradation and can be monitored using InSAR satellite technology. We combined InSAR data, processed using the ASPIS algorithm to monitor ground motion between 2017 and 2021, with airborne optical and LiDAR data to investigate the rate of subsidence across palsa peatlands in northern Sweden. We show that 55% of Sweden's eight largest palsa peatlands are currently subsiding, which can be attributed to underlain permafrost landforms and their degradation. The most rapid degradation occured in the largest palsa complexes in the most northern part of the region of study, also corresponding to the areas with the highest % palsa cover within the overall mapped wetland area. Further, higher degradation rates were found in areas where winter precipitation has increased substantially. The roughness index calculated from a LiDAR-derived DEM, used as a proxy for degradation, increases alongside subsidence rates and may be used as a complementary proxy for palsa degradation. We show that combining datasets captured using remote sensing enables regional-scale estimation of ongoing permafrost degradation, an important step towards estimating the future impact of climate change on permafrost-dependent ecosystems.

Keywords: Permafrost, subsidence, Arctic, InSAR, palsa, peatlands

1.0 Introduction

Permafrost regions are critical components in the climate system, due to their essential carbon (C) storage service (Harris et al., 2022). The circumpolar permafrost region in particular, stores around 1300±200 Pg of organic C, corresponding to around 50% of the global terrestrial C pool (Hugelius et al., 2020; Köchy et al., 2015). It covers around 21 million km^2 or 22% of the Northern Hemisphere's exposed land surface (Obu, 2021). Northern peatlands themselves store an estimated 415±150 Pg of C in an area covering around 3.7 million km^2 of which around 1.7 million km^2 is permafrost within the circumpolar permafrost region in discontinuous and sporadic permafrost zones (Hugelius et al., 2020). Permafrost in these peatlands raises the surface above the water table forming so-called palsa (pl. palsas) or, in extended form, peat plateaux (Seppälä, 2011). These account for substantial areas of global permafrost, including in northern Fennoscandia (Ballantyne., 2018; Gisnås et al., 2017; Tarnocai et al., 2009). In northern Sweden, 137 km^2 of these palsa have been recorded from field reports (Backe, 2014). Climate warming, and the associated alteration in the precipitation regime, is increasingly recognized to be a particular threat to permafrost (Biskaborn et al., 2019), with the subarctic Fennoscandian permafrost region, and the palsa within, particularly vulnerable (Christiansen et al., 2010; Farbrot et al., 2013).

Modelling studies project unsuitable conditions for permafrost within the coming century, with the most pessimistic estimates projecting unsuitability even sooner - by 2040 in Fennoscandia (Chadburn et al., 2017; Fewster et al., 2022; Könönen et al., 2022; Stefan et al., 2006). As palsa are often found in the sporadic or discontinuous permafrost zone (Zuidhoff & Kolstrup, 2000), they are particularly sensitive to climate warming and any resultant permafrost thaw and disappearance. Their sensitivity mainly results from the alterations in the thermal insulation effect of peat deposits and snow as the climate changes (Seppälä, 2011; Smith & Riseborough, 1996). Specifically, organic peat has a high thermal conductivity when wet and frozen, but low conductivity when dry and thawed. Snow has a highly insulating effect on ground temperature. Thus, extended periods of air-temperatures below 0°C and thin snow cover in winter are beneficial to maintain or grow the perennial frozen core of palsas and peat plateaux. Low summer precipitation, which reduces the thermal conductivity of peat, also helps to preserve the frozen cores in palsa. In contrast, increased snowfall has been linked to permafrost degradation as it increases winter insulation. Further, high summer precipitation leads to higher thermal conductivity of peat, and combined with warm summer temperatures, can degrade permafrost by increasing permafrost temperatures and subsequent thawing of the frozen peat core of palsas. The strong insulating properties of peat allow the occurrence of permafrost at the southern extent of the northern permafrost region and valley bottoms in areas otherwise too warm for permafrost (Johansson et al., 2013; Seppälä, 2011; Smith & Riseborough, 1996).

Warming of the permafrost in palsa typically leads at the surface, to top-down thaw, (i.e. thickening of the active layer), and eventual subsidence of the surface, as well as lateral thaw, sometimes called abrupt thaw or thermokarst, which occurs at the margin of peat plateaux and palsa edges (Seppälä, 2011; Smith & Riseborough, 1996; Zuidhoff, 2002). This is often associated with water-logged conditions and, as a result, increased methane (CH$_4$) emissions (Glagolev et al., 2011; Hugelius et al., 2020; Matthews et al., 1997; Miglovets et al., 2021; Schuur et al., 2009; Turetsky et al., 2020; Varner et al., 2022), which is a central theme for permafrost research (Sjöberg *et al.*, 2020). A subsequent impact of this permafrost degradation is an alteration in vegetation cover, its hydrology, and human use of the landscape (e.g., infrastructure and reindeer husbandry)(Markkula et al., 2019; Ramage et al., 2021). Given the potentially large impacts of permafrost thaw on the global climate, ecosystem function and human activity, quantification and monitoring of the subsidence in peat deposits affected by permafrost thaw and degradation, as well as an understanding of their sensitivity to changing climatic parameters, is urgently required (IPCC, 2021).

The degradation of the permafrost of palsas has been observed right across the circumpolar permafrost region in a number of studies, including in northern Scandinavia (Åkerman & Johansson, 2008; de la Barreda-Bautista et al., 2022; Luoto & Seppälä, 2003; Olvmo et al., 2020; Sannel et al., 2016; Varner et al., 2022); Russia (Glagolev et al., 2011; Miglovets et al., 2021; van Huissteden et al., 2021); the USA (Douglas et al., 2021; Douglas et al.,

84 2015; Sannel, 2020) and Canada (Mamet et al., 2017; Sannel & Kuhry, 2011; Short et al., 2014; Vallée &
85 Payette, 2007). Although rapid degradation in response to short term climatic events has been observed,
86 typically permafrost degradation has been investigated via long-term monitoring at decadal timescales in
87 response to changes in temperature and precipitation conditions (Åkerman & Johansson, 2008; de la Barreda-
88 Bautista et al., 2022; Olvmo et al., 2020; Sannel et al., 2016). These longer-term studies have shown strong
89 relationships between permafrost degradation and summer temperatures, length of the thaw period, winter
90 precipitation and snow depth (Smith et al., 2022). These types of analyses are very useful for quantifying how
91 much of the landscape has already transitioned and understanding the climate change drivers behind these
92 changes, but they do not capture the initial stages of permafrost degradation in palsas and the lower rates of
93 subsidence that have yet to result in observable changes in the vegetation or thermokarst formation. The latter is
94 crucial to understand the ongoing response of palsas to climate warming and to predict when pulses of
95 greenhouse gases to the atmosphere and other impacts (e.g., on infrastructure) are likely to occur. Thus, we need
96 approaches that detect early signs of degradation at landscape scales, with repeated observations.

97 Due to the vast extent and remoteness of permafrost areas there is no current complete annual degradation rate
98 measurements. So, we looked to satellite remote sensing to underpin the measurement and monitoring
99 assessment of permafrost peatlands, their degradation and resultant climate impacts (Hugelius et al., 2020;
100 Swingedouw et al., 2020). Optical remote sensing approaches can be augmented with RaDAR remote sensing
101 methods, including InSAR, to capture the early response of permafrost to warming. These methods can detect
102 vertical land surface motion at millimetre precision across a range of natural landscapes, with greater confidence
103 in the direction of surface motion than the absolute magnitude (Alshammari et al., 2020; Alshammari et al.,
104 2018; Bartsch *et al.*, 2016; de la Barreda-Bautista et al., 2022; Short et al., 2014; van Huissteden et al., 2021).
105 The regular sampling frequency, insensitivity to cloud and, in the case of Sentinel-1, low cost, means InSAR
106 from Sentinel-1 should be well suited to measure and monitor ongoing changes in permafrost affected by
107 climate change. Further, Sentinel-1 for InSAR is effective at both local and regional scales - the 20m × 20m
108 spatial resolution enables measurement of surface motion within local sites (de la Barreda-Bautista et al., 2022),
109 and can do so over entire and complex landscapes, such as the circumpolar permafrost region (Reinosch et al.,
110 2020).

111 The overall aim of this study was to carry out a regional-scale analysis of permafrost degradation across the
112 palsas of northern Sweden, principally using Sentinel-1 InSAR-derived subsidence as an indication of
113 degradation. Pertinent to this is that any InSAR-detected changes can be associated with known and delineated
114 targets in the wider landscape. Furthermore, it is also important to understand any within-site dynamics of
115 permafrost degradation. This paper therefore has specific objectives to: (i) measure the subsidence rate between
116 2017-2021 of all major palsa complexes in the northern Sweden region; (ii) determine in which palsa complexes
117 subsidence is greatest, and (iii) assess if the spatial patterns of degradation can be linked to climatic variables
118 and properties of the different sites across the region. To achieve these objectives, we combined large-scale
119 regional analysis with higher resolution site-specific analysis of patterns in subsidence, using a combination of
120 datasets - satellite (Sentinel-1) InSAR; occupied airborne optical and LiDAR data; and snow depth,
121 precipitation, and temperature time-series from meteorological stations across the region.

2.0 Methodology

2.1 Study area

This study focused on the northern part of Sweden; a region containing palsa, located between 68.84-67.64° N and 18.71-21.19° E. The palsas of the region are confined predominantly to valley bottoms in an elevation range between ca. 350 and 590m asl (Fig. 1). The rest of the study area region is comprised of forests and/or mountain land covers (Siewert, 2018; Åkerman & Johansson, 2008). Of all the palsas in the region, the eight largest complexes of concentrated palsa range between 50 and 273ha in area (Table 1). These were located across the region, which covers a ca. 20,000km² area, with the largest palsa sites located north-west. Smaller palsas occur scattered in distribution right across the region. The climate varies from north to south (www.smhi.se). The mean January and July temperatures in Karesuando in the northern part is -16 and 12.8°C, respectively, while in Kiruna, slightly further south, the mean January, and July temperatures is -11.6 and 13.4C (1991-2020 average). Mean annual precipitation is 443 and 560mm in Karesuando and Kiruna, respectively.
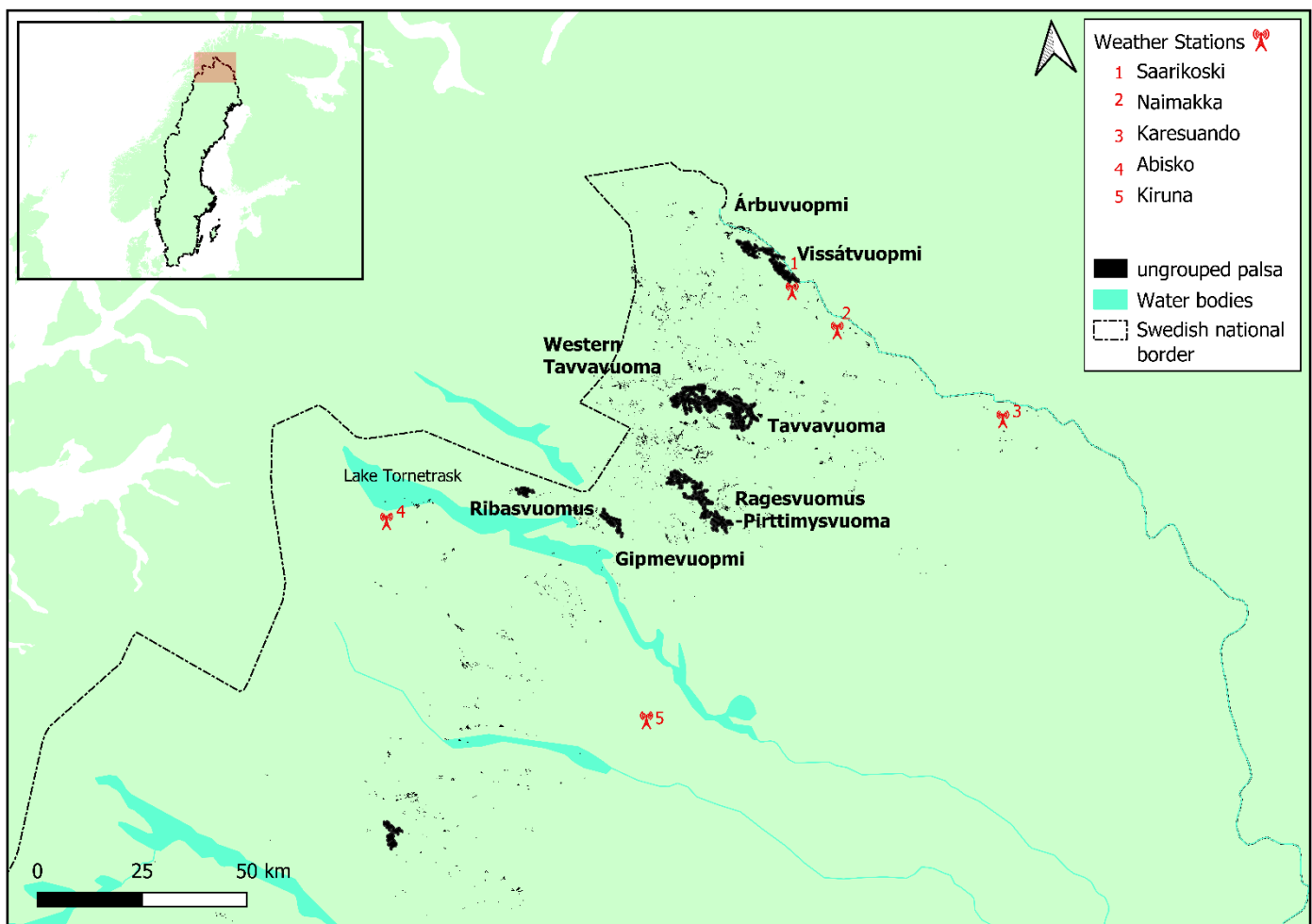
Figure. 1: Map of the palsa in Sweden which were investigated in the study focusing on the eight named palsa complexes. The black regions show all the palsa which has been reported to exist (Backe, 2014,) with the larger named areas displaying the 250m buffers around the palsa areas which have created continuous expanses. Meteorological station positions used in the study are also indicated.

A previous national palsa mapping dataset provided raster cells at a spatial resolution of 100m, with the % palsa cover computed and a 250m buffered output to provide continuous palsa area outputs (Backe, 2014). This afforded analyses at a spatial resolution suitable for analysis with Sentinel-1 yet provide practical representation of the condition of the palsa in this region. All these data were analysed in this study, but the eight largest

143 continuous areas of these palsa (Backe, 2014) were focused on, hereon in referred to as palsa
144 complexes, a term reflecting their mosaic nature of raised palsa and/or peatland plateaux, interspersed with lower lying fen or
145 thermokarst areas. These eight sites account for the majority of the palsa areas in Sweden, the sites are listed in
146 Table 1 along with some associated information on their status and total and raised palsa plateaux areas.

147

148 *Table. 1: Information on the major palsa complexes analysed in this paper (Backe, 2014). The protection status*
149 *means no or limited direct anthropogenic activities that may influence palsa degradation. Total site area is*
150 *calculated from the total number of 100m × 100m palsa pixels at each site - these pixels have associated*
151 *percentages for how much of the 100m x 100m area is palsa. The average of these percentages for each site*
152 *displays the palsa density at each site. These percentages are then used to calculate the "total palsa area" for*
153 *each site based on the original report estimates.*

Site Name	Protection Classification	Total site area (ha)	Average extent palsa in these areas (%)	Total palsa area (ha)	LiDAR Collection year	Central location (Latitude, Longitude)
Árbuvuopmi	Not protected	327	26.3	86.06	2018, 2016	21.03464, 68.83842
Vissátvuopmi	Not protected	867	31.6	273.75	2015, 2018	21.19497, 68.79412
Tavvavuoma	EU Natura 2000 SPA, SAC. Site of National Importance for Nature conservation	1719	15.8	271.25	2018	20.85043, 68.51132
Western Tavvavuoma	EU Natura 2000 SPA, SAC. Site of National Importance for Nature conservation	813	13.0	105.74	2018	20.57727, 68.53953
Gipmevuopmi	Pristine mountain forest, Nature reserve, EU Natura 2000 SCI	303	23.0	69.62	2013	20.09767, 68.28377
Ragesvuomus-Pirttimysvuoma	Pristine mountain forest, Nature reserve, EU Natura 2000 SCI	881	6.55	57.74	2013	20.48660, 68.3741
Sirccam	EU Natura 2000 SCI	397	12.8	50.70	2015	18.71528, 67.64537
Ribasvuomus	Pristine mountain forest, Nature reserve, EU Natura 2000 SCI	216	23.2	50.13	2014	19.60100, 68.36116

154

155 2.2 Datasets

156 The InSAR-derived dataset of surface motion over this northern Sweden region of study was calculated for the
157 period between 2017 to 2021, from single look complex (SLC) C-band SAR data, captured in Interferometric
158 Wide (IW) Swath mode by the Sentinel-1 constellation (European Union's Copernicus Programme; Torres et al.,
159 2012). SAR data input were from the thaw season when there was minimal coverage of snow and ice (i.e., between
160 April and October in each year). Data from descending tracks 168 and 66 were used to cover the target area. Four
161 stacks were processed independently with one from track 168 and three from track 66, which was split into a
162 northern, middle, and southern subsets. The APSIS (formerly ISBAS) method (Sowter et al., 2013; Sowter et al.,
163 2016) was used to characterize surface motion which relaxes the need for consistent phase stability and therefore
164 enables near-complete spatial and temporal coverage over vegetated surfaces (Alshammari et al., 2020;
165 Alshammari et al., 2018; Bradley et al., 2022; Cigna & Sowter, 2017; Gee et al., 2017; Sowter et al., 2016),
166 including those found across snow-free permafrost regions.

167 InSAR processing of Sentinel-1 IW SLC imagery involves a series of steps summarised in Figure 2. Firstly,
168 deburst and merging involved combining individual sub-swaths into a single wide-area SLC product. Secondly,
169 the process of deramping produced a product where the problem of an ambiguous and rapidly changing phase
170 with azimuth was solved for; a specific deramping function is available for Sentinel-1 data (ESA, 2015). Next
171 step involved the co-registration of each Sentinel-1 image to a common slant range coordinate system and multi-

172 looking of data by factors of 5 m in range and 20 m by azimuth. This produced a dataset with an approximate
173 spatial resolution of 20m × 20m. Using a perpendicular baseline of 250m and maximum temporal baseline of 183
174 days ∼ 2100 interferograms were generated per stack. The temporal baseline was chosen to balance the need to
175 reduce the baseline to minimise phase ambiguities and best maintain coherence across the region, whilst also using
176 a baseline long enough to generate season-to-season pairs over consecutive years. This is required over permafrost
177 regions to capture more subtle trends of surface motion during the thaw period (de la Barreda-Bautista et al., 2022;
178 Liu et al., 2010). The interferograms were unwrapped using a modified version of the SNAPHU algorithm (Shen
179 et al., 2002), which converts circular phase data into a linear measure of deformation. The algorithm was modified
180 in order to allow the ability to parallelise and to spread the calculation across multiple cores (Chen and Zebker,
181 2002). The multi-annual average velocity was calculated for pixels which maintained a coherence greater than
182 0.45 in a minimum of ∼ 650 interferograms, with respect to stable reference points located in the town Kautekenio
183 (N˚69.00, E˚23.04) for track 168 and Narvik (N˚68.44, E˚17.42), Kvikkjokk (N˚66.95, E˚17.72), and Rognan
184 (N˚67.09) for the subsets of track 66. The line-of-sight measurements were converted to vertical surface
185 displacement using a cosine correction and finally mosaicked into a single deformation product. Localised UAV
186 studies at sites in Sweden have verified the ability to use InSAR as a tool to monitor permafrost degradation (de
187 la Barreda-Bautista et al., 2022).
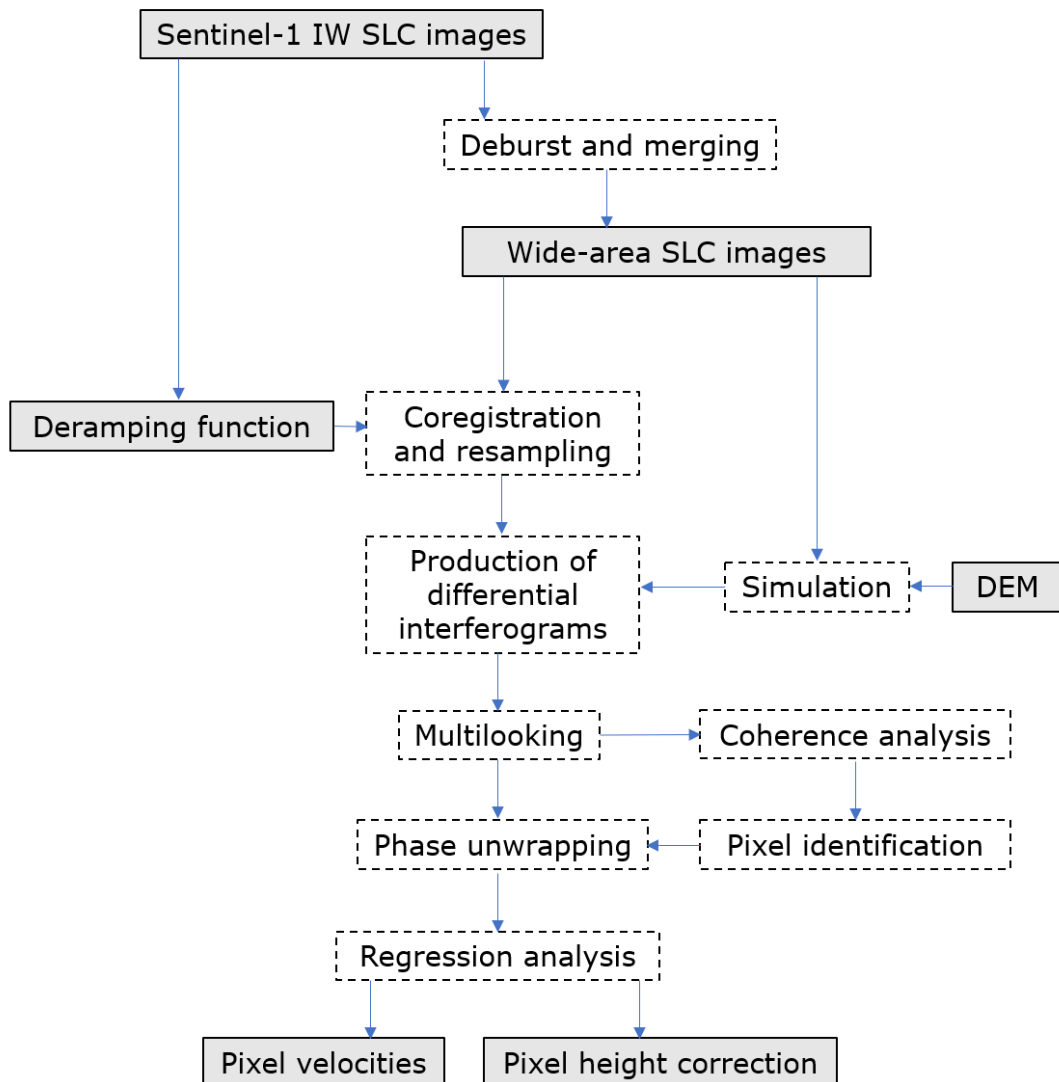
188

189 *Figure 2: A flowchart summarising the steps undertaken for InSAR processing using the APSIS method to create*
190 *a surface motion product from Sentinel-1 IW SLC imagery. Boxes shaded grey represent data sets, boxes with*
191 *dotted borders represent processing steps. Modified from Sowter et al. (2016).*

In order to interpret the resultant surface motion dataset produced by the ASPIS InSAR method, two sets of additional data were sourced: (i) higher resolution remote sensing data and (ii) meteorological data. The former included orthophotos captured of the eight target areas by occupied airborne surveys commissioned by the Swedish Mapping, Cadastral and Land Registration Authority (www.lantmateriet.se; © Lantmäteriet). The orthophotos (Lantmäteriet, 2021) have scenes covering a 5km × 5km area, at a 0.5m spatial resolution, the majority were captured in 2021, although gaps were filled with imagery from 2018 for two sites. The Swedish National Digital Elevation Model (DEM), was also used in this study. The DEM was derived via occupied airborne LiDAR data capture between 2013 and 2018 (Table 1) processed to compute elevation at 2m spatial resolution across Sweden (www.lantmateriet.se; © Lantmäteriet). The orthophotos and DEM provided elevation and landscape characteristics (geomorphic features) for use in this study. The meteorological data was captured by the Swedish Metrological and Hydrological Institute (www.smhi.se) at meteorological stations across the region. Specifically, the air temperature, precipitation, and snow depth data, were sourced and used from specific stations, i.e., those located closest to the palsa complexes under investigation namely at Abisko, Kiruna, Karesuando, Saarikoski, and Naimakka (Fig. 1).

2.3 Data analyses

2.3.1 Surface motion statistics

The ASPIS InSAR surface motion dataset was clipped to the 100m x 100m spatial resolution of the whole palsa dataset and separately to the eight palsa complexes (Backe, 2014). From this the frequency distributions of ASPIS InSAR surface motion at these eight palsa complexes, and over all individual palsa peatland raster cells in the region, were produced. Using these data, the maximum and minimum rates of surface motion at each site was determined, as well as the sum of the pixels with palsas that showed subsidence. These derived data relating to surface motion were further interpreted using the orthophotos and DEMs, supported by the meteorological data.

2.3.2 Roughness thresholds

The DEM tiles were joined together and clipped to the eight palsa complexes. Following this, the degree of elevation roughness was calculated, via the native topographic roughness index function (Riley, DeGloria, & Elliot, 1999). This roughness index was thresholded at > 0.5 to provide a visual depiction of palsa landform edges in the otherwise typically even terrain of the valley bottoms where the palsas occur. The roughness data was visually compared to the orthophotos from a subset of areas to assess its potential for delineating palsas and this allowed us to determine a threshold value that connected these continuous terrain variables to the specific features of the palsa complexes, such as the raised mound structure of the palsa – so-called palsa mounds (Franklin, 2020). Hillshade was also calculated via the native QGIS function using the default formula, which uses a lighting effect to visualise the roughness of the terrain from differences in local elevation (QGIS, 2022). The roughness, hillshade, and elevation outputs were overlaid on the mapped palsa tiles to provide higher resolution visual interpretation.

2.3.3. Causes of surface motion

To test for the causes of surface motion palsa ASPIS InSAR surface motion was compared against roughness, elevation and palsa percentage provided with the palsa raster cells (Backe, 2014). The roughness, elevation and InSAR outputs were resampled to the resolution of the mapped palsa tiles (100m x 100m) to enable statistical comparison. The zonal statistics tool was used to extract mean average values from the resulting roughness and elevation outputs for the 100m spatial resolution mapped palsa tiles.

To analyse the relationships between surface motion, roughness and percent palsa in each 100m by 100m pixel stratified by palsa complex, SciPy statistics (Virtanen et al., 2020) was used to obtain Pearson's correlation statistics with an alpha value of 0.05 used to test for significance. Pandas (McKinney, 2011) and NumPy (Harris et al., 2020) were used for data management. All scripts are available on the project GitHub (https://github.com/SamValman/Permafrost_Sweden).

238   2.3.4 Climatic factors

239   Mean annual, maximum, and minimum daily air temperature, precipitation, and depth of ground snow for the
240   period 2000 to 2022 from the meteorological station nearest to a correspondent palsa complex were extracted and
241   analysed. The Naimakka station did not record snow depth and the Saarikoski station did not record air
242   temperature, however, it was deemed that at the regional scale of this study these sites were sufficiently close
243   together (18km) to be interchangeable. Subsequently, data was averaged to provide an annual measurement of
244   each meteorological variable for each station/palsa complex. Due to incomplete meteorological datasets, a longer-
245   term record of the meteorological variables was not possible for all sites. However, long-term climate data
246   (>100years) was available from three meteorological stations in the region: namely, Karesuando, Kiruna, and
247   Abisko. This data was used to assess temporal variability in annual, winter (December, January, and February
248   (DJF)) and summer (June, July, and August (JJA)) temperature, precipitation and snowfall since the start of
249   records across the region. Descriptive statistics (mean, minimum, maximum and inter-quartile range) were
250   produced to express the regional differences between these sites. Lastly, to complement the point based
251   meteorological (both weather and climate) data, we used modelled permafrost probabilities based on climatic
252   conditions to explore relationships between climatic conditions (Obu et al., 2018) and subsidence rates. In this
253   context, it is worth noting that there may be a mismatch between the modelled permafrost distribution and
254   permafrost in palsa areas as this can, in some areas, be a relic of cooler climatic conditions. We used the mean
255   values from the roughness and InSAR data to resample to 100m spatial resolution in line with the permafrost
256   raster cells and spatially joined the permafrost probability layer, taking the mean value where the 100m cell
257   straddled multiple permafrost probability cells.

258   The relationship between the meteorological variables both over the last two decades at the weather stations
259   closest to the palsa complexes and duration of the climate record at the three weather stations with the longest
260   data series were assessed using linear regression analysis in Genstat (VNS Ldt). Assumptions of normality and
261   homogeneity of variance of the residuals were assessed using residual plots in Genstat. Some of time series were
262   incomplete, in these instances the analysis was conducted using the slightly shorter time series (see fig. 8).

263

264   **3.0 Results**

265   3.1 Surface motion

266   The ASPIS InSAR-derived surface motion outputs for the time-period of interest (2017-2021), ranged
267   between -9.9 and 7.7mm yr^{-1} across all of the palsa raster cells measured in northern Sweden, with a mean of 0.05,
268   median of 0.2 and range of 17.7mm yr^{-1}. Focusing solely on the eight palsa complexes provided greater insight
269   and excluded the most extreme uplift values from scattered individual palsas (Table 2). 69% of results were within
270   MSE of changing ground motion direction.

271   *Table. 2: InSAR subsidence and uplift measurements of the palsa complexes defined in Figure 1 and Table 1.*
272   *The total palsa area were used to isolate and extract ASPIS InSAR measurements of surface motion at each of*
273   *the eight sites.*

Site	Max subsidence (mm yr^{-1})	Max uplift (mm yr^{-1})	Subsiding area (ha)	Area subsiding >3.5 mm yr^{-1} (ha)	Mean standard error (mm yr^{-1})
Árbuvuopmi	-9.9	1.7	321.3	138.4	1.5
Vissátvuopmi	-8.9	3.5	796.2	204.8	1.5
Tavvavuoma Western	-6.4	6.6	1009.4	50.9	1.4
Tavvavuoma	-5.1	6.3	215.0	1.0	1.4
Gipmevuopmi	-6.9	6.3	117.2	1.8	1.2
Ragesvuomus-Pirttimysvuoma	-5.9	5.7	358.6	7.4	1.4
Sirccam	-3.1	5.4	135.3	0.0	0.9
Ribasvuomus	-6.5	5.5	93.6	0.7	1.3

274

275

The spatial plots of surface motion for each palsa complex displayed in Figure 3, illustrates patterns of surface motion (both subsidence and uplift and associated variance) across this northern Sweden region. This is evident both within the palsa complexes and between the complexes.
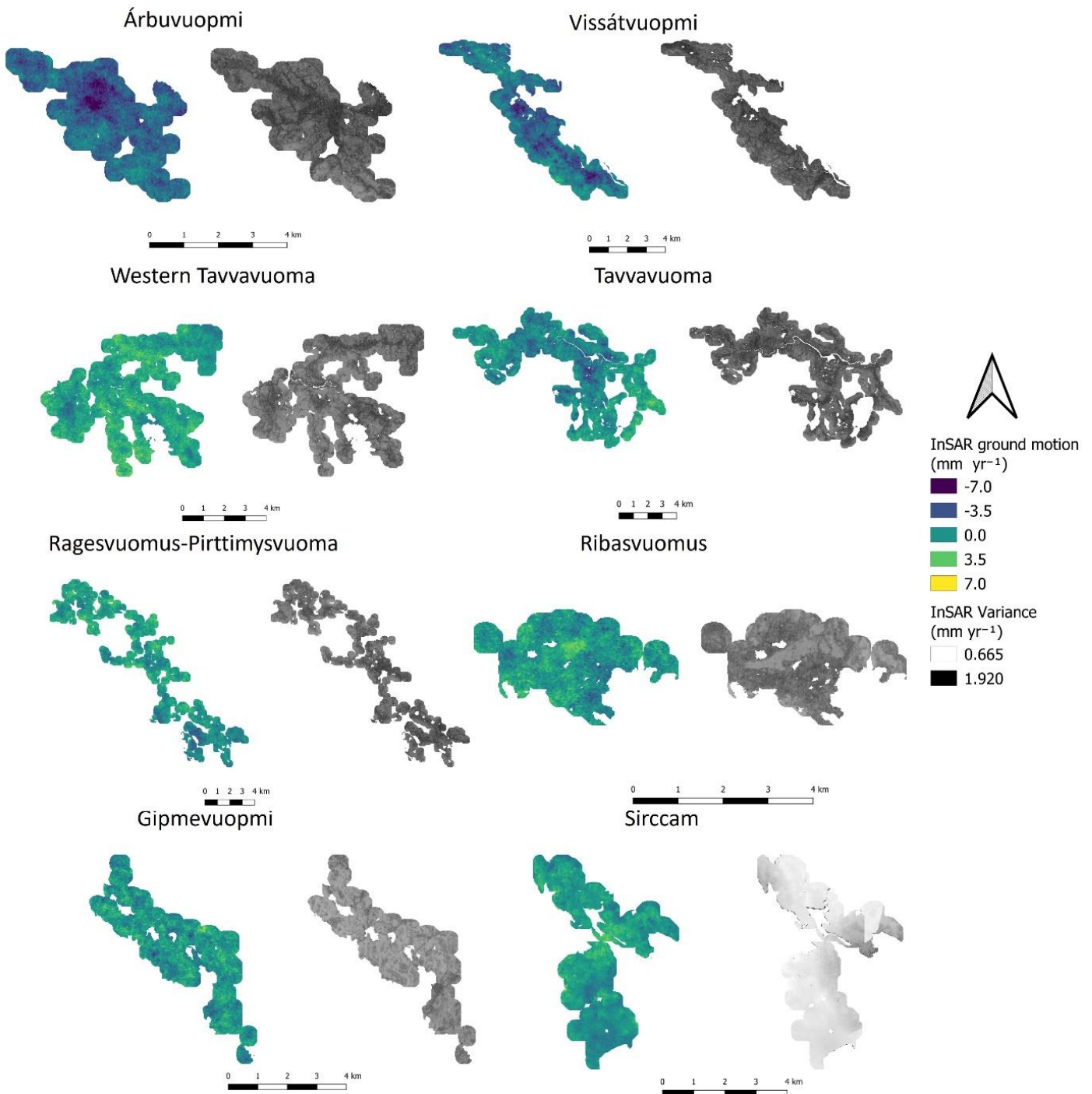
Figure. 3: Palsa ground motion measured using Satellite InSAR from 2017 to 2021, showing differing levels of degradation across the eight study sites. Sites are ordered by their latitudinal position. Negative values correspond to subsidence. Note that in order to plot continuous areas the scenes shown are the palsa area plus a 250m buffer around each 100m ×100m raster cell that cover a minimum of 1% palsa (Backe 2014). This means that areas of non-palsa peatland and some areas with mineral soil are included in the figure. ASPIS InSAR variance were less than 1.5mm yr^{-1} in over 90% of pixels.

286 Across the target sites 3046.6ha (Table 2) out of the total site area of 5523ha (Table 1) were subsiding, which
287 equates to ca 55% of the total palsa complexes' area. Out of the subsiding parts of the palsa complexes, 405ha
288 were subsiding at rates >3.5mm yr^{-1} at near gaussian distribution. However, it is evident from the frequency
289 distribution plots, that it is in the palsa complexes in the far north of the region that subsidence dominated the
290 surface motion measured (Table 2, Fig. 4). At Vissátvuompi and Árbuvuopmi 98 and 92% of the palsa complexes
291 were subsiding with maximum subsidence rates of -9.9 and -8.9mm yr^{-1}, respectively. The measured area affected
292 by high subsidence rates of between (>3.5mm yr^{-1}) were 204.8ha and 138.4ha at Vissátvuompi and Árbuvuopmi,
293 respectively. This means that ca. 30% of the total combined area of these two sites (1194ha) is in the highest range
294 of subsidence. The high degree of palsa subsidence at Vissátvuompi and Árbuvuopmi was confirmed by field
295 observations at these sites (Sofie Sjogersten, pers. Obs.): Both sites showed signs of active lateral erosions, large
296 scale subsidence and thermokarst formation. The more southerly sites also show subsidence, although ground
297 motion rates were much more stable, with the -1 and 1mm yr^{-1} range being most common (Fig. 4). Areas further
298 to the south and west showed signs of uplift, particularly the western parts of Tavvavuoma and Ribasvuomus with
299 maximum rates of uplift of 6.3mm across some smaller parts of these sites. However, all sites have some degree
300 of subsidence, albeit at a lower rate compared to the heavily subsiding northern sites.

301
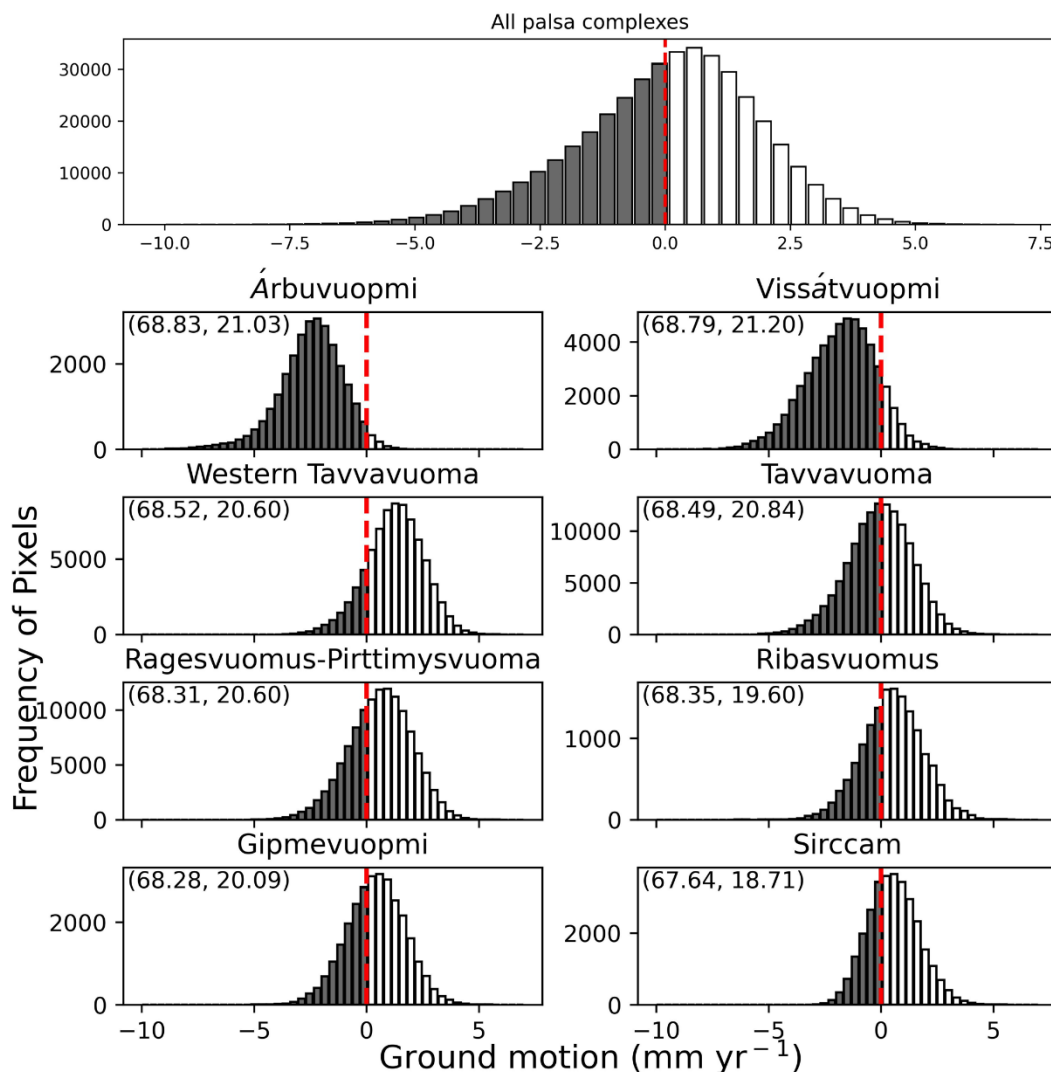
302

303 *Figure. 4: Distribution of 20m ×20m ASPIS InSAR pixels within each of the palsa complexes in this study and*
304 *the overall trend of the dataset according to the distribution of pixel moving in a particular direct and a given*
305 *rate. Shaded areas with negative values correspond to subsidence. The dashed central lines indicate pixels in*
306 *stable areas with no motion. Central point latitude and longitude is provided for each site in brackets for each*
307 *site.*

3.2 Topographic drivers and indicators

Calculating the roughness index from the DEMs at each palsa complex enabled differentiation of palsa from surrounding lower lying and flat fen areas. Representative example complexes are shown in Figures 5 and 6 - Vissátvuopmi and Western Tavvavuoma, Overall, the palsa complexes to the north (e.g., Fig. 5b, c) display a more pronounced topography across the focus areas than the more south-westerly ones (e.g., Fig. 6b, c). There was clear correspondence between density of palsa and subsidence, i.e., areas with more palsa showed more subsidence (Fig. 5a, d). Furthermore, the palsa complexes showed greater elevation variation compared to surrounding fen areas and were more densely clustered to the north than in the more south westerly sites. These features spatially coincided with higher subsidence. Substantial within site variability in subsidence was evident, where the pixels with the highest subsidence rates being clustered together and following landscapes features, e.g., palsa plateaux edges. It was evident that many separate palsa complexes in an area resulted in a high degree of elevation change, causing a high roughness index. In turn, areas with high roughness have the greatest subsidence (Fig. 5,6). Visual comparison between orthophotos and roughness showed that areas of high roughness corresponded well with areas of severe permafrost degradation (as indicated by lateral erosion and thermokarst formation).
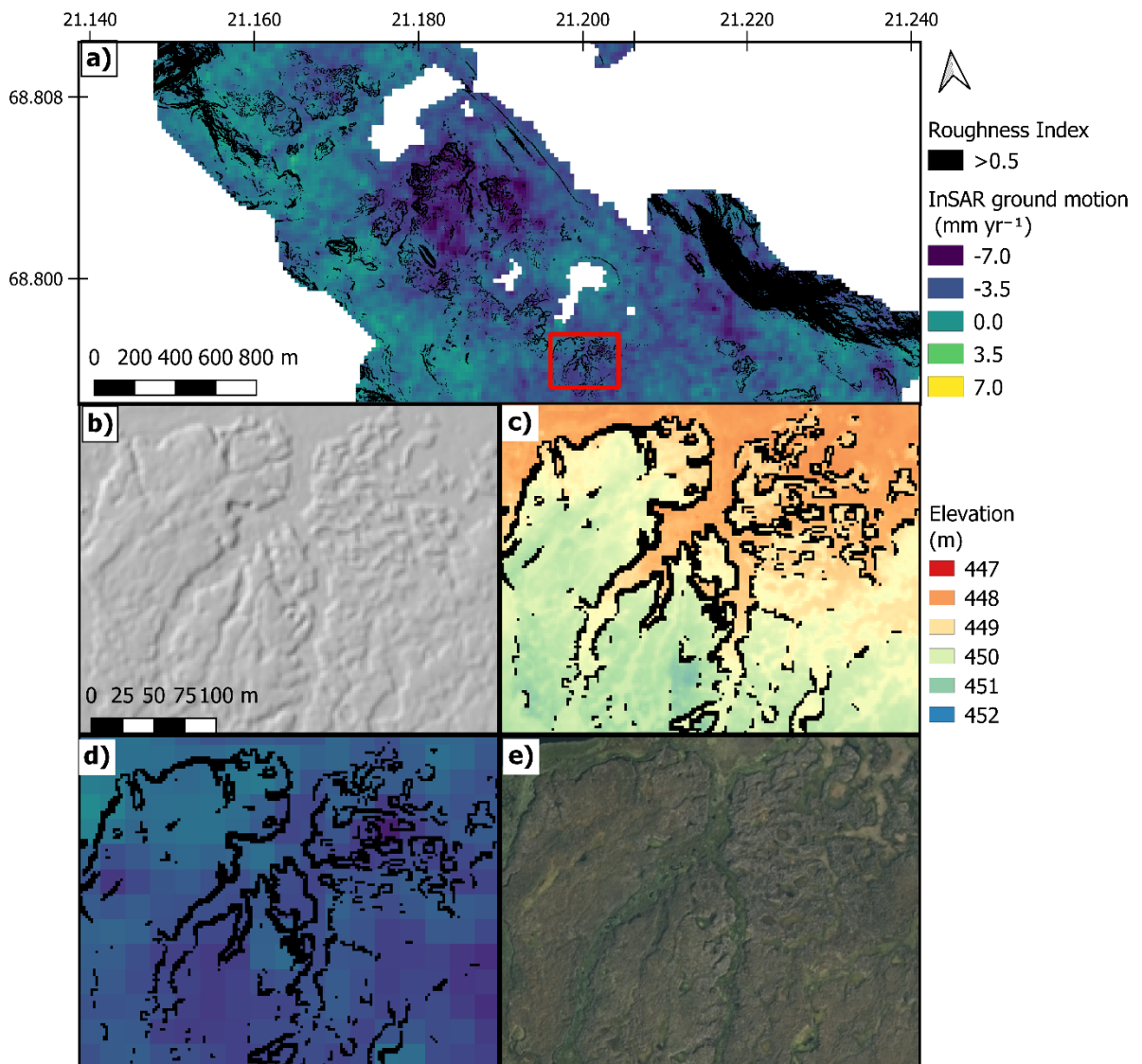
Figure. 5: Visual analysis of Vissátvuopmi one of the sites where the most subsidence was found to be occurring. Evaluation of correspondence of hillshade DEM (b), DEM (c) and a close look at InSAR subsidence (d) with palsa complexes suggested by roughness overlays and aerial imagery (e). The positioning of b,c, and d within the larger site (a) show bands of subsidence proximal to roughness patches suggesting palsa.
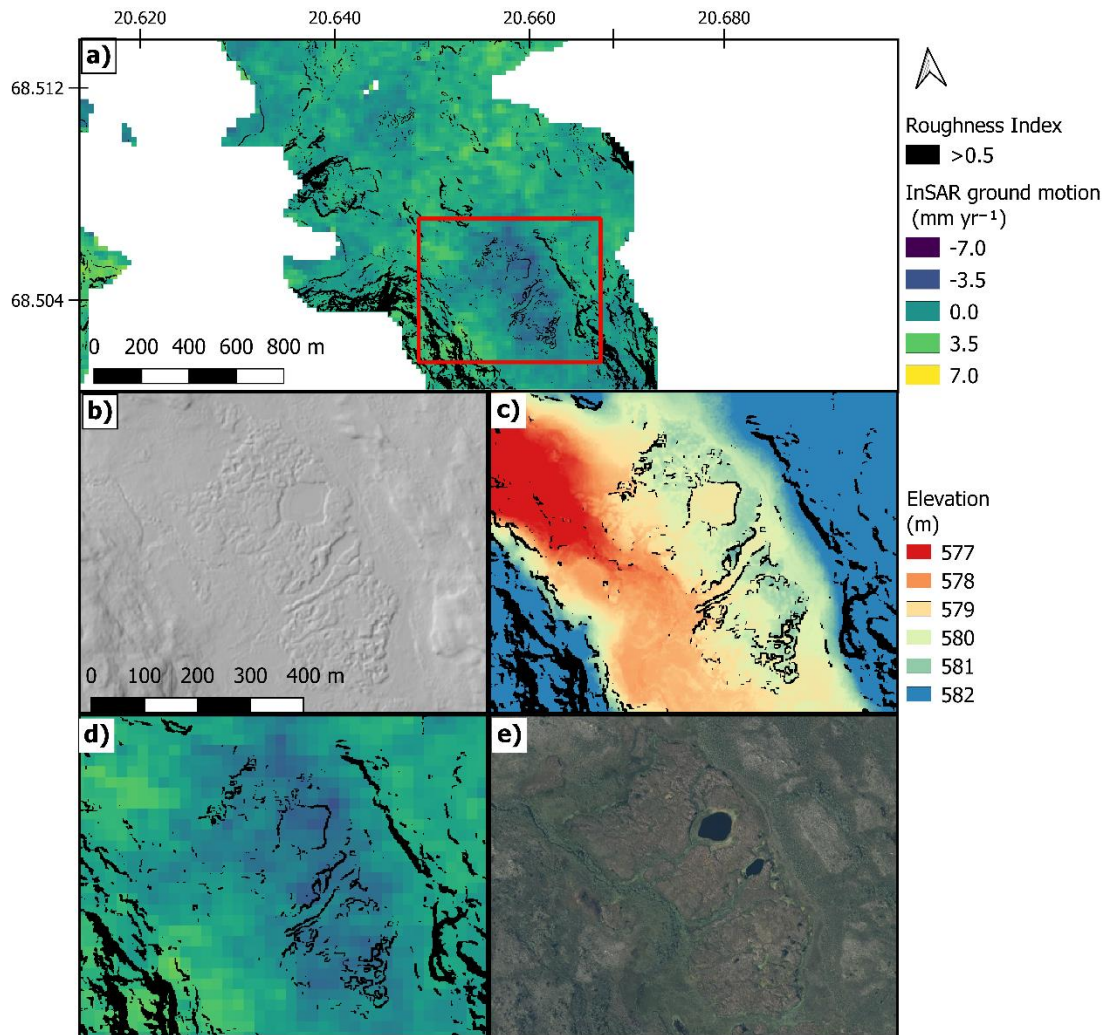
329
330 *Figure. 6: Visual analysis of Tavvavuoma which was found to have much lower levels of subsidence in*
331 *comparison to more northern sites. Evaluation of correspondence of hillshade DEM (b), DEM (c) and InSAR*
332 *subsidence (d) with Palsa complexes suggested by roughness overlays and aerial imagery (e). The positioning*
333 *of b,c, and d within the larger site (a) show many less "bands" (linear arrangements of palsa across the image)*
334 *of subsidence and potential palsa than Figure 4.*
335

336 Regression analysis showed a relationship between roughness and subsidence as sites with greater subsidence
337 were also found to have greater roughness (Fig. 7a). Higher percentage palsa in a location was linearly related to
338 subsidence with the greatest subsidence found in areas with the highest percentage palsa cover (Fig. 7b). It was
339 also clear that the modelled permafrost probability did not correspond to the percentage of palsa, i.e. pixels with
340 100% palsa are in some instances predicted to have no permafrost (Fig. 7b).

341
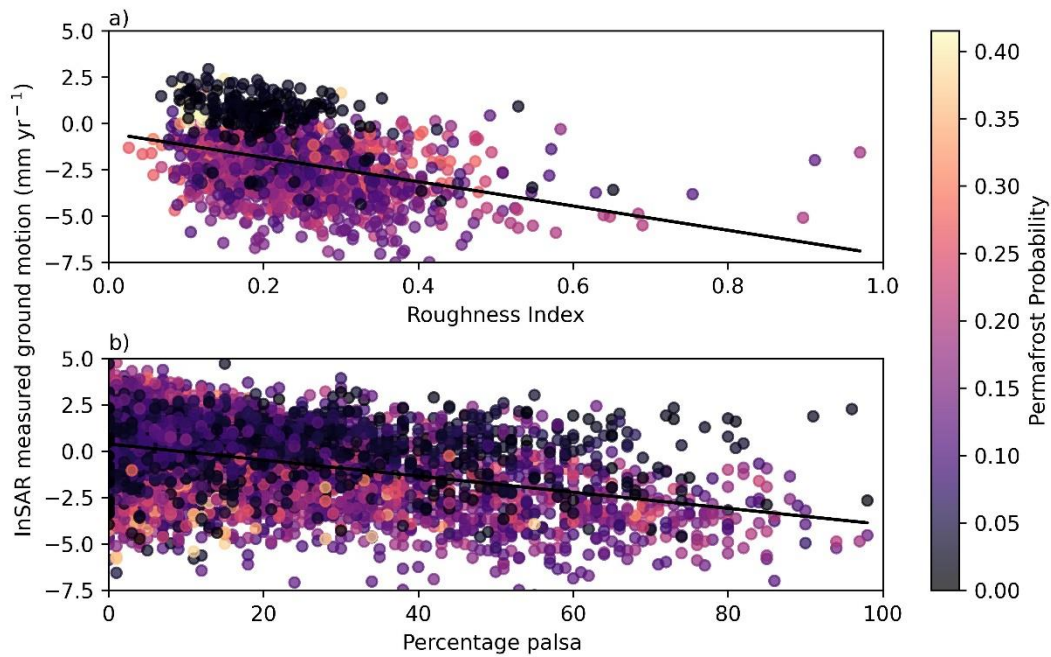
Figure. 7: Relationship between a) the roughness index; p < 0.001, R² = 0.35 and b) percentage palsa in a pixel; p < 0.001, R² = 0.41 and subsidence. The colours indicated for each data point are the analysed probability (on a scale from 0 to 1) that an area would include permafrost, (Obu et al., 2018). Note that there is less data for the analysis of roughness as the roughness was characterized only for the eight study sites and not all palsa raster cells from (Backe, 2014). Roughness values from valley sides (which at time were included in the buffer areas) are not used in the figure.

3.4 Meteorological trends

The analysis of the meteorological data showed variability in both weather and climate across the study region in part reflecting the patterns in the subsidence data. The warmest minimum and maximum temperatures, -29.2 and 32.8ºC respectively, were recorded for the palsa complexes north of Lake Tornetrask, i.e. Gipmevuomi and Ribasvuomus (Abisko weather station) (Fig. 1). The temperature in the area of Árbuvuopmi, Vissátvuopmi, and Tavvavuoma palsa complexes (Saarikoski/Naimaka and Karesuando weather stations) ranged between -39.4 and 30.5ºC (Table 3, Fig. 8a). The sites had comparable annual snow depth with a mean of 20-30cm (Table 3, Fig. 8b).
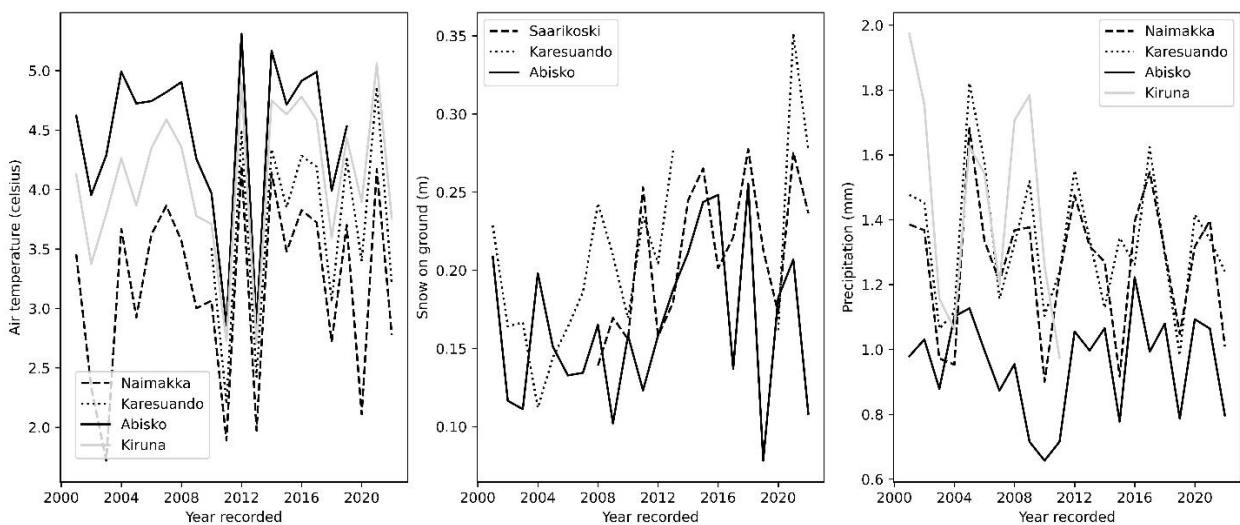
356
357 *Figure. 8: Mean annual a) daily maximum temperature, b) snow depth on the ground, and c) daily precipitation at the meteorological stations in the study region (SMHI 2022).*

Table. 3: Temperature and snowfall descriptive statistics. The snow depth data are estimated from days with snow on the ground. Mean annual temperature and precipitation are averaged from 2000 to 2021. Maximum, minimum and the inter-quartile range are of daily maximum temperature and daily precipitation since 2000 are also shown. Some weather stations lack certain years but were considered to have adequate coverage for this task while two sites did not have sufficient data collection during the time period to be reliable and were shaded out.

Weather Station	Temperature (°C)				Snow depth (m)			Precipitation (mm)		
	Mean annual	Max daily	Min daily	IQR daily	Mean annual	Max daily	IQR daily	Mean annual	Max daily	IQR daily
Naimakka	-1.40	29.5	-38.2	15.7				456	50.8	1.0
Saarikoski					76.9	0.85	0.43	422	43.6	0.9
Karesuando	-0.70	30.5	-39.4	16.9	75.1	1.00	0.40	490	53.2	1.1
Abisko	0.53	32.8	-29.2	13.5	60.0	1.27	0.42	348	61.9	0.6
Kiruna	0.06	30.3	-30.6	15.6	5.3	1.13	0.45	545	53.1	0.9

There was no detectable difference in climatic trends among the meteorological weather stations since 2001 for any of these sites ($p > 0.05$). In contrast, the longer-term climate records show a strong increase in winter precipitation over the last 140 years at Karesuando, the northern most weather station of the three with long term records available ($F_{1,136}=122.33$, $p < 0.001$; $\sigma^2=47.0$ %; Fig. 9a). This long-term trend was also evident, albeit less strong, in Kiruna ($F_{1,110} = 28.17$, $p < 0.001$; $\sigma^2=19.7$ %; Fig. 9b). In Abisko, the pattern of increasing in winter (DJF) precipitation was less clear ($F_{1,108}=8.29$, $p < 0.01$; $\sigma^2=6.3$ %; Fig. 9c). Mean annual Snow depth, temperature, and summer precipitation (JJA) did not show clear temporal trends (See supplementary materials).
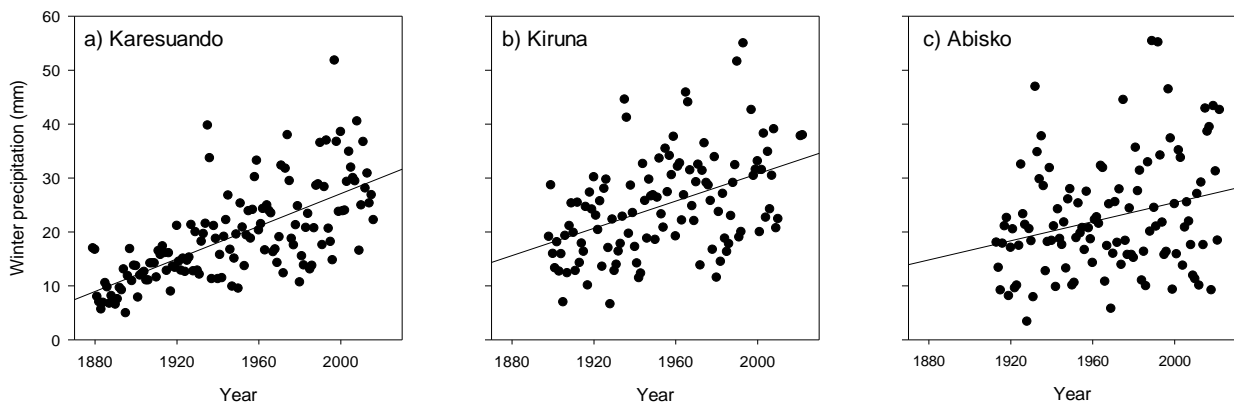
Figure 9. Mean winter (DJF) precipitation over time at a) Karesuando, b) Kiruna, and c) Abisko, significant trendlines are shown.

4. Discussion

By way of satellite ASPIS InSAR-derived surface motion and associated spatial and statistical analyses, we have demonstrated on-going subsidence in the palsas of northern Sweden driven by a warming climate. Based on the compelling agreement of subsidence with palsa landforms and their roughness, we interpret this as permafrost degradation, i.e., thaw of the permafrost core within palsas and disintegration of these landforms. This is in line with a wide range of literature (see introduction) and concurs with the local-scale studies in the area undertaken using both satellite- and field-based methods (de la Barreda-Bautista et al., 2022; Olvmo et al., 2020; Sannel, 2020; Sannel et al., 2016; Sannel & Kuhry, 2011). The findings also agree with what is expected from the severe climate warming impacts on temperatures and precipitation noted in the region (Hänsel, 2020;

389 Irannezhad et al., 2017; Vikhamar-Schuler et al., 2016) and the modelled predictions of total loss of permafrost
390 across the region within decades (Fewster et al., 2022). We suggest that the surface subsidence of the sample
391 palsa complexes measured in this study, together with complementary work in Norway (Borge et al., 2017), can
392 be taken as evidence of substantial permafrost degradation in many palsa areas across northern Sweden and
393 therefore, likely to be also occurring across northern Fennoscandia

394 The processes driving the degradation of the permafrost, as measured by the ASPIS InSAR-derived subsidence
395 data, are complex. Although permafrost degradation was observed in all the palsa complexes, rates varied both
396 within and among palsa complexes (Table 2, Fig. 3 and 4). Overall, the InSAR subsidence data demonstrates a
397 south to north gradient in increasing degradation. This indicates that local factors, such as local climate warming
398 responses or permafrost temperature, determine the sensitivity of particular areas and that regional climatic
399 gradients play a role in the long-term trajectory of these ecosystems (Johansson et al., 2011; Olvmo et al., 2020).
400 In particular, winter precipitation is generally considered a strong predictor of permafrost degradation due to the
401 highly insulating properties of snow, preventing heat dissipation during winter (Olvmo et al., 2020; Seppälä,
402 2011). This points to increased winter precipitation in the part of the northern most part of study areas as a
403 driver of the higher subsidence rates at the northern most palsa complexes (Table 2 and Fig. 8a). Interestingly,
404 climate data from the last two decades did not reveal strong differences in climatic conditions over the area. This
405 suggests that long-term trends combined with a buffered system reaction to change are driving regional patterns
406 in permafrost degradation.

407 It could also be the case that the observed north to south gradient of subsidence rates reflect different phases of
408 progression in an ongoing trend of permafrost degradation across the study region of northern Sweden. It is
409 plausible that the degradation process has progressed further at the more southern sites, reflecting higher
410 permafrost temperatures, and that as a result, subsidence rates have now slowed. All the while at the northern
411 sites, which still have a high cover of palsa: 26.3 and 31.6 % at Árbuvuopmi and Vissátvuopmi respectively,
412 show high subsidence rates. This is supported by research showing rapid permafrost degradation in the
413 southernmost palsa complexes in Sweden (Zuidhoff, 2002; Zuidhoff & Kolstrup, 2000) and in the area around
414 and to the south of Tornetrask, since the 1960's (Åkerman & Johansson, 2008; de la Barreda-Bautista et al.,
415 2022; Varner et al., 2022). However, permafrost degradation in palsas have progressed over longer-time periods
416 even in northern Fennoscandia. Here palsas' have decreased in areal extent by 33– 71% over ca. 60 years, with
417 more rapid contraction in recent years in Finmarkvidda, Norway and 54% in Vissátvuopmi, northern most
418 Sweden (Borge et al., 2017; Olvmo et al., 2020) and total loss of palsa complexes has been recorded in the far
419 north eastern parts of Norway (Vorren 2017).

420 Although there are differences in subsidence rates among sites the region wide permafrost degradation reflects
421 ongoing climatic trends (Fig. 3 and 7). Since 1901 Fennoscandia's climate has become wetter as well as warmer
422 with a greater proportion of the precipitation falling as rain relatively to snow (Hänsel, 2020; Irannezhad et al.,
423 2018; Irannezhad et al., 2017; Vikhamar-Schuler et al., 2016). These trends are reflected in the far north where
424 higher air temperatures, greater precipitation and snow depths has already shifted climatic conditions, in parts of
425 the region, away from those that support permafrost in peatlands e.g. since the 1940's (Åkerman & Johansson,
426 2008; Borge et al., 2017; Olvmo et al., 2020). Further, deep permafrost boreholes show decadal signals of
427 increasing temperatures in the Scandes mountains suggesting that warmer temperatures have been impacting
428 permafrost since the 1920's (Isaksen et al., 2007). Hence, is seems that climate warming has been impacting
429 permafrost in Fennoscandia for at least 100 years.

430 As a result of the ongoing trend of increasing permafrost temperatures in palsas in Fennoscandia, their
431 permafrost temperatures are now close to $0^{o}C$, making them especially vulnerable to decay in response to
432 further increases in temperatures (Christiansen et al., 2010; Farbrot et al., 2013). Palsa formation is closely
433 linked to the mean annual temperature, with temperatures below -1 to $-2^{o}C$ and limited insulating snow cover
434 over consecutive years needed as a threshold for palsas to form (Vorren, 2017). In this context it is important to
435 note that the MAT in the area was between 0.53 and $-1.4^{o}C$ since 2000 suggesting that at least in parts of the
436 study area the climatic conditions do not support formation of palsa anymore while conditions are marginal for
437 palsa preservation in the entire region.

438 Although subsidence dominated in the northern sites, uplift was also noted in the study region. Mechanisms that
439 may explain patterns of uplift are formation of new palsa as well as short-lived frost mounds that can form
440 temporarily in the palsa system (Zuidhoff, 2002). Further mechanisms that may result in uplift are changes in
441 the water level of the flooded parts of the peatlands as well as accumulation of plant residues from the

442 productive fen vegetation parts of the study sites on the peatland surface, reflecting adaptation of the local
443 ecosystem to degraded palsa mounds reflected by changes in remotely sensed terrain surface.

444 In addition to demonstrating regional permafrost degradation in northern Fennoscandia, this work also provides
445 proof of concept for circumpolar assessments of permafrost degradation using ASPIS InSAR. It enables
446 detection of the areas with rapidly degrading permafrost and deepening active layers but also peat consolidation
447 in areas that have already lost its permafrost (de la Barreda-Bautista et al., 2022). The fact that InSAR data is
448 integrated over 20m × 20m pixels means that the signal of local level degradation may be somewhat dampened
449 (de la Barreda-Bautista et al., 2022). However, the high precision of the change in vertical position means that
450 InSAR is an important tool to employ to detect the initial stages of large-scale permafrost degradation. In
451 concurrence with the literature (Alshammari et al., 2020; Alshammari et al., 2018; Bartsch *et al.*, 2016; de la
452 Barreda-Bautista et al., 2022; Short et al., 2014; van Huissteden et al., 2021), we found the majority (69%) of
453 our results were within the MSE of direction of ground motion change, providing confidence to locate where
454 permafrost is degrading. Currently, the study of long-term trends and drivers using InSAR is somewhat limited
455 by the short collection period of Sentinel 1, but as more data are continued to be collected, methods such as non-
456 linear time series creation will become viable to compare subsidence directly to longer climatic drivers.
457 However, our large-scale assessment of permafrost subsidence provides a baseline to direct, and compare,
458 against future fieldwork monitoring in northern Sweden.

459 As a complement to the ASPIS-InSAR data, the novel roughness thresholding method used here together with
460 contextual data proved a powerful tool to map and monitor changes (Franklin, 2020; Konig et al., 2019; Otto et
461 al., 2012). This approach could be developed using machine learning methods to model palsa dynamics to better
462 automate the extraction of palsa landform positions (Konig et al., 2019; Luoto & Seppälä, 2002). If
463 accomplished, the operating extent of this tool could be vastly increased using the Arctic 2m DEM dataset over
464 area were its quality is high enough to allow high resolution mapping of the degrading edges of raised palsa
465 plateaux (Morin, 2016; Karlson et al., 2021). In turn this could be used to remove the stable centre of palsa
466 plateaux and exclusively compare palsa edges to the roughness index, where we would expect to find a stronger
467 correlation than there exists with the current palsa raster cells (Fig. 7a). It has been suggested that small,
468 fragmented, and irregularly shaped palsa are more susceptible to erosion (Borge et al., 2017; Mamet et al., 2017,
469 Beer et al. in review). We have not gone as far as to estimate this here but the possible palsa edges inferred from
470 the roughness index, could be built upon for this understanding. Casual analysis of figures 5, 6 and the
471 orthophotos provided in the supplementary materials would support these expectations. Together the ASPIS-
472 InSAR and the DEM derived roughness index metrics offer novel ways of large scale monitoring of permafrost
473 degradation. This will help to quantify the rate of palsa ecosystem collapse and transition to a non-permafrost
474 state.

475 We conclude that permafrost degradation of palsas is occurring across northern Sweden, with the greatest rates
476 of degradation and largest areas impacted being Sweden's two largest palsa complexes in the far north. This
477 raises serious concerns that these systems will lose their permafrost entirely in the coming decades especially as
478 climatic conditions are approaching the limits of sustaining palsa (Fewster et al., 2022). The implications of this
479 rapid loss of permafrost is ecosystem collapse and loss, as the permafrost core is fundamental to the existence of
480 palsa. Future research should focus on the implications of this collapse on increased CH_4 emissions (Glagolev *et*
481 *al.*, 2011; Turetsky *et al.*, 2020; Varner *et al.*, 2022),carbon loss (Hugelius *et al.*, 2020), and thus the potential
482 for strong climate feedbacks (IPCC, 2021) as well as using longer-time InSAR data as this becomes available to
483 investigate regional variations in climatic drivers of permafrost degradation. Further, our study demonstrates
484 that InSAR together with terrain data can be applied over continuous natural surfaces at a regional-scale to
485 monitor permafrost degradation in palsa, offering a tool for circumpolar monitoring of climate warming impact
486 on these systems.

487

488 **5. Acknowledgement**

489 This work was supported by funding from the University of Nottingham, UK, EU-InterAct funding via the
490 InterAccess programme and the Swedish research council (VR-2021-05767 to M. Siewert). Associated
491 fieldwork was supported by the Climate Impacts Research Centre (CIRC) at Umeå University. Samuel Valman
492 was supported by the EPSRC funded Geospatial Centre for Doctoral Training (EP/S023577/1).

6. Author contributions

SV: Carried out the majority of the data analysis and made a significant contribution to data interpretation, writing and finalising the manuscript text. Both SV and MS can be considered to have contributed equally to this work.

MS: Contributed to the conception of the study, contributed DEM and orthophoto data, carried out fieldwork to assess permafrost degradation, contributed and advised on data analysis and interpretation, contributed to structuring, writing, and refining the text. Both MS and SV can be considered to have contributed equally to this work.

DB: Contributed to the conception of the study, advised on the data analysis, and made a significant contribution to finalising the text.

ML: Provided data analysis, support on the InSAR processing, data interpretation, and writing of the text.

DG: Carried out the initial InSAR data processing

BBB: Contributed to the conception of the study and refining the text.

AS: Contributed to the conception of the study and advised on the InSAR data processing

SS: Conceived and directed the study, contributed to data analysis, carried out fieldwork to assess permafrost degradation and made a significant contribution to formulating and finalising the text.

SS, DB, AS and MS secured the funding for the project.

Code Availability

All the python scripts used to carry out these analyses are available at the github repository:
https://github.com/SamValman/Permafrost_Sweden.

Data Availability statement

The Sentinel-1 datasets are freely available and can be obtained by searching and downloading the Interferometric Wide (IW) swath mode products for orbit track numbers 168 and 66 through the Copernicus Open Access Hub (https://scihub. copernicus.eu/dhus/#/home). The processed interferometric data and deformation maps are commercially sensitive and may be made available on reasonable request by email addressed to the corresponding author. All other datasets produced during this project will be uploaded on zenodo and the DOI provided once the article has been accepted.

References

Åkerman, H. J., & Johansson, M. (2008). Thawing permafrost and thicker active layers in sub-arctic Sweden. *Permafrost and Periglacial Processes*, *19*(3), 279-292. https://doi.org/10.1002/ppp.626

Alshammari, L., Boyd, D. S., Sowter, A., Marshall, C., Andersen, R., Gilbert, P., Marsh, S., & Large, D. J. (2020). Use of Surface Motion Characteristics Determined by InSAR to Assess Peatland Condition [https://doi.org/10.1029/2018JG004953]. *Journal of Geophysical Research: Biogeosciences*, *125*(1), e2018JG004953. https://doi.org/https://doi.org/10.1029/2018JG004953

Alshammari, L., Large, D. J., Boyd, D. S., Sowter, A., Anderson, R., Andersen, R., & Marsh, S. (2018). Long-Term Peatland Condition Assessment via Surface Motion Monitoring Using the ISBAS DInSAR Technique over the Flow Country, Scotland. *Remote Sensing*, *10*(7). https://doi.org/10.3390/rs10071103

Armstrong McKay, D. I., Staal, A., Abrams, J. F., Winkelmann, R., Sakschewski, B., Loriani, S., Fetzer, I., Cornell, S. E., Rockström, J., & Lenton, T. M. (2022). Exceeding 1.5°C global warming could trigger multiple climate tipping points. *Science*, *377*(6611), eabn7950. https://doi.org/doi:10.1126/science.abn7950

Backe, S. (2014). *Kartering av Sveriges palsmyrar*. Länsstyrelsen.

Ballantyne C. K. (2018). *Periglacial geomorphology*. John Wiley & Sons.

Bartsch, A., Widhalm, B., Kuhry, P., Hugelius, G., Palmtag, J., Siewert, M.B., 2016. Can C-band synthetic aperture radar be used to estimate soil organic carbon storage in tundra? *Biogeosciences*, 13, 5453-5470.

Beer, J. M., Wang, Y., Way, R., Forget, A. & Colyn, V. 2023. Uncrewed aerial vehicle-based assessments of peatland permafrost vulnerability along the Labrador Sea coastline, northern Canada.

Biskaborn, B. K., Smith, S. L., Noetzli, J., Matthes, H., Vieira, G., Streletskiy, D. A., Schoeneich, P., Romanovsky, V. E., Lewkowicz, A. G., Abramov, A., Allard, M., Boike, J., Cable, W. L., Christiansen, H. H., Delaloye, R., Diekmann, B., Drozdov, D., Etzelmüller, B., Grosse, G., . . . Lantuit, H. (2019). Permafrost is warming at a global scale. *Nature Communications*, *10*(1), 264. https://doi.org/10.1038/s41467-018-08240-4

Borge, A. F., Westermann, S., Solheim, I., & Etzelmüller, B. (2017). Strong degradation of palsas and peat plateaus in northern Norway during the last 60 years. *The Cryosphere*, *11*(1), 1-16. https://doi.org/10.5194/tc-11-1-2017

Bradley, A. V., Andersen, R., Marshall, C., Sowter, A., & Large, D. J. (2022). Identification of typical ecohydrological behaviours using InSAR allows landscape-scale mapping of peatland condition. *Earth Surf. Dynam.*, *10*(2), 261-277. https://doi.org/10.5194/esurf-10-261-2022

Chadburn, S. E., Burke, E. J., Cox, P. M., Friedlingstein, P., Hugelius, G., & Westermann, S. (2017). An observation-based constraint on permafrost loss as a function of global warming. *Nature Climate Change*, *7*(5), 340-344. https://doi.org/10.1038/nclimate3262

Chen, C.W. and Zebker, H.A., 2001. Two-dimensional phase unwrapping with use of statistical models for cost functions in nonlinear optimization. JOSA A, 18(2), pp.338-351.

Christiansen, H. H., Etzelmüller, B., Isaksen, K., Juliussen, H., Farbrot, H., Humlum, O., Johansson, M., Ingeman-Nielsen, T., Kristensen, L., Hjort, J., Holmlund, P., Sannel, A. B. K., Sigsgaard, C., Åkerman, H. J., Foged, N., Blikra, L. H., Pernosky, M. A., & Ødegård, R. S. (2010). The thermal state of permafrost in the nordic area during the international polar year 2007–2009. *Permafrost and Periglacial Processes*, *21*(2), 156-181. https://doi.org/https://doi.org/10.1002/ppp.687

Cigna, F., & Sowter, A. (2017). The relationship between intermittent coherence and precision of ISBAS InSAR ground motion velocities: ERS-1/2 case studies in the UK. *Remote Sensing of Environment*, *202*, 177-198. https://doi.org/https://doi.org/10.1016/j.rse.2017.05.016

de la Barreda-Bautista, B., Boyd, D. S., Ledger, M., Siewert, M. B., Chandler, C., Bradley, A. V., Gee, D., Large, D. J., Olofsson, J., Sowter, A., & Sjögersten, S. (2022). Towards a Monitoring Approach for Understanding Permafrost Degradation and Linked Subsidence in Arctic Peatlands. *Remote Sensing*, *14*(3). https:// doi.org/10.3390/rs14030444

Douglas, T. A., Hiemstra, C. A., Anderson, J. E., Barbato, R. A., Bjella, K. L., Deeb, E. J., Gelvin, A. B., Nelsen, P. E., Newman, S. D., Saari, S. P., & Wagner, A. M. (2021). Recent degradation of interior Alaska permafrost mapped with ground surveys, geophysics, deep drilling, and repeat airborne lidar. *The Cryosphere*, *15*(8), 3555-3575. https://doi.org/10.5194/tc-15-3555-2021

Douglas, T. A., Jorgenson, M. T., Brown, D. R. N., Campbell, S. W., Hiemstra, C. A., Saari, S. P., Bjella, K., & Liljedahl, A. K. (2015). Degrading permafrost mapped with electrical resistivity tomography, airborne imagery and LiDAR, and seasonal thaw measurements. *GEOPHYSICS*, *81*(1), WA71-WA85. https://doi.org/10.1190/geo2015-0149.1

582 ESA (2015). Definition of the TOPS SLC deramping function for products generated by the S-1 IPF. *European*
583   *Space Agency*. COPE-GSEG-EOPG-TN-14-0025, Issue 1, Revision 2, 22 April 2015.
584 Farbrot, H., Isaksen, K., Etzelmüller, B., & Gisnås, K. (2013). Ground Thermal Regime and Permafrost
585   Distribution under a Changing Climate in Northern Norway. *Permafrost and Periglacial Processes*,
586   *24*(1), 20-38. https://doi.org/https://doi.org/10.1002/ppp.1763
587 Fewster, R. E., Morris, P. J., Ivanovic, R. F., Swindles, G. T., Peregon, A. M., & Smith, C. J. (2022). Imminent
588   loss of climate space for permafrost peatlands in Europe and Western Siberia. *Nature Climate Change*,
589   *12*(4), 373-379. https://doi.org/10.1038/s41558-022-01296-7
590 Franklin, S. E. (2020). Interpretation and use of geomorphometry in remote sensing: a guide and review of
591   integrated applications. *International Journal of Remote Sensing*, *41*(19), 7700-7733.
592   https://doi.org/10.1080/01431161.2020.1792577
593 Fronzek, S., Luoto, M., & Carter, T. (2006). Potential effect of climate change on the distribution of palsa mires
594   in subarctic Fennoscandia. *Climate Research*, *32*(1), 1-12. https://www.int-
595   res.com/abstracts/cr/v32/n1/p1-12/
596 Gee, D., Bateson, L., Sowter, A., Grebby, S., Novellino, A., Cigna, F., Marsh, S., Banton, C., & Wyatt, L.
597   (2017). Ground Motion in Areas of Abandoned Mining: Application of the Intermittent SBAS (ISBAS)
598   to the Northumberland and Durham Coalfield, UK. *Geosciences*, *7*(3).
599   https://doi.org/10.3390/geosciences7030085
600 Gisnås, K., Etzelmüller, B., Lussana, C., Hjort, J., Sannel, A. B. K., Isaksen, K., Westermann, S., Kuhry, P.,
601   Christiansen, H. H., Frampton, A., & Åkerman, J. (2017). Permafrost Map for Norway, Sweden and
602   Finland. *Permafrost and Periglacial Processes*, *28*(2), 359-378.
603   https://doi.org/https://doi.org/10.1002/ppp.1922
604 Glagolev, M., Kleptsova, I., Filippov, I., Maksyutov, S., & Machida, T. (2011). Regional methane emission
605   from West Siberia mire landscapes. *Environmental Research Letters*, *6*(4), 045214.
606 Hänsel, S. (2020). Changes in the Characteristics of Dry and Wet Periods in Europe (1851–2015). *Atmosphere*,
607   *11*(10), 1080. https://www.mdpi.com/2073-4433/11/10/1080
608 Harris, C. R., Millman, K. J., van der Walt, S. J., Gommers, R., Virtanen, P., Cournapeau, D., Wieser, E.,
609   Taylor, J., Berg, S., Smith, N. J., Kern, R., Picus, M., Hoyer, S., van Kerkwijk, M. H., Brett, M.,
610   Haldane, A., del Río, J. F., Wiebe, M., Peterson, P., . . . Oliphant, T. E. (2020). Array programming
611   with NumPy. *Nature*, *585*(7825), 357-362. https://doi.org/10.1038/s41586-020-2649-2
612 Harris, L. I., Richardson, K., Bona, K. A., Davidson, S. J., Finkelstein, S. A., Garneau, M., McLaughlin, J.,
613   Nwaishi, F., Olefeldt, D., Packalen, M., Roulet, N. T., Southee, F. M., Strack, M., Webster, K. L.,
614   Wilkinson, S. L., & Ray, J. C. (2022). The essential carbon service provided by northern peatlands.
615   *Frontiers in Ecology and the Environment*, *20*(4), 222-230.
616   https://doi.org/https://doi.org/10.1002/fee.2437
617 Hugelius, G. A., Loisel, J. A., Chadburn, S. A., Jackson, R. A., Jones, M. A., MacDonald, G., Marushchak, M.,
618   Olefeldt, D. A., Packalen, M., Siewert, M. A.., Treat, C. A.-O., Turetsky, M., Voigt, C. A., & Yu, Z. A.
619   (2020). Large stocks of peatland carbon and nitrogen are vulnerable to permafrost thaw. *Proceedings of*
620   *the National Academy of Sciences*, 117(34), 20438-20446. https://doi.org/10.1073/pnas.1916387117.
621 IPCC. (2021). *The Physical Science Basis. Contribution of Working Group I to the Sixth Assessment Report of*
622   *the Intergovernmental Panel on Climate Change*. Cambridge University Press.
623 Irannezhad, M., Moradkhani, H., & Kløve, B. (2018). Spatiotemporal Variability and Trends in Extreme
624   Temperature Events in Finland over the Recent Decades: Influence of Northern Hemisphere
625   Teleconnection Patterns. *Advances in Meteorology*, *2018*, 7169840.
626   https://doi.org/10.1155/2018/7169840
627 Irannezhad, M., Ronkanen, A.-K., Kiani, S., Chen, D., & Kløve, B. (2017). Long-term variability and trends in
628   annual snowfall/total precipitation ratio in Finland and the role of atmospheric circulation patterns.
629   *Cold Regions Science and Technology*, *143*, 23-31.
630   https://doi.org/https://doi.org/10.1016/j.coldregions.2017.08.008
631 Isaksen, K., Sollid, J. L., Holmlund, P., & Harris, C. (2007). Recent warming of mountain permafrost in
632   Svalbard and Scandinavia. *Journal of Geophysical Research: Earth Surface*, *112*(F2).
633   https://doi.org/https://doi.org/10.1029/2006JF000522
634 Johansson, M., Åkerman, J., Keuper, F., Christensen, T. R., Lantuit, H., & Callaghan, T. V. (2011). Past and
635   Present Permafrost Temperatures in the Abisko Area: Redrilling of Boreholes. *AMBIO*, *40*(6), 558.
636   https://doi.org/10.1007/s13280-011-0163-3
637 Johansson, M., Callaghan, T. V., Bosiö, J., Åkerman, H. J., Jackowicz-Korczynski, M., & Christensen, T. R.
638   (2013). Rapid responses of permafrost and vegetation to experimentally increased snow cover in sub-
639   arctic Sweden. *Environmental Research Letters*, *8*(3), 035025. https://doi.org/10.1088/1748-
640   9326/8/3/035025

641 Karlson, M., bastviken, D. & reese, H. (2021). Error characteristics of pan-arctic digital elevation
642   models and elevation derivatives in northern sweden. *Remote Sensing,* 13**,** 4653.

643 Köchy, M., Hiederer, R., & Freibauer, A. (2015). Global distribution of soil organic carbon – Part 1: Masses and
644   frequency distributions of SOC stocks for the tropics, permafrost regions, wetlands, and the world.
645   *SOIL*, *1*(1), 351-365. https://doi.org/10.5194/soil-1-351-2015

646 König, S., Schultz, J. A., Schoch, A., Blöthe, J., Schrott, L., & Thonfeld, F. (2019). Mountain Permafrost
647   Distribution Modeling–A Geomorphometry-Remote Sensing Approach for the Hohe Tauern National
648   Park, Austria. *Dreiländertagung der DGPF, der OVG und der SGPF in Wien, Österreich–*
649   *Publikationen der DGPF*, 28.

650 Könönen, O. H., Karjalainen, O., Aalto, J., Luoto, M., & Hjort, J. (2022). Environmental spaces for palsas and
651   peat plateaus are disappearing at a circumpolar scale. *The Cryosphere Discuss.*, *2022*, 1-37.
652   https://doi.org/10.5194/tc-2022-135

653 Lantmäteriet. (2021). Orthophoto (Ortofoto) [Online]. Version 2.7. Available at:
654   https://www.lantmateriet.se/globalassets/geodata/geodataprodukter/flyg--och-
655   satellitbilder/e_pb_ortofoto.pdf. Accessed on 10th January 2024.

656 Liu, L., Zhang, T., & Wahr, J. (2010). InSAR measurements of surface deformation over permafrost on the
657   North Slope of Alaska. *Journal of Geophysical Research: Earth Surface*, *115*(F3).
658   https://doi.org/10.1029/2009JF001547

659 Luoto, M., & Seppälä, M. (2002). Modelling the distribution of palsas in Finnish Lapland with logistic
660   regression and GIS. *Permafrost and Periglacial Processes*, *13*(1), 17-28.

661 Luoto, M., & Seppälä, M. (2003). Thermokarst ponds as indicators of the former distribution of palsas in
662   Finnish Lapland. *Permafrost and Periglacial Processes*, *14*(1), 19-27. https://doi.org/10.1002/ppp.441

663 Mamet, S. D., Chun, K. P., Kershaw, G. G. L., Loranty, M. M., & Kershaw, G. P. (2017). Recent Increases in
664   Permafrost Thaw Rates and Areal Loss of Palsas in the Western Northwest Territories, Canada.
665   *Permafrost and Periglacial Processes*, *28*, 619-633. https://doi.org/ 10.1002/ppp.1951

666 Markkula, I., Turunen, M., & Rasmus, S. (2019). A review of climate change impacts on the ecosystem services
667   in the Saami Homeland in Finland. *Science of The Total Environment*, *692*, 1070-1085.
668   https://doi.org/https://doi.org/10.1016/j.scitotenv.2019.07.272

669 Matthews, J. A., Dahl, S.-O., Berrisford, M. S., & Nesje, A. (1997). Cyclic Development and Thermokarstic
670   Degradation of Palsas in the Mid-Alpine Zone at Leirpullan, Dovrefjell, Southern Norway. *Permafrost*
671   *and Periglacial Processes*, *8*(1), 107-122. https://doi.org/https://doi.org/10.1002/(SICI)1099-
672   1530(199701)8:1<107::AID-PPP237>3.0.CO;2-Z

673 McKinney, W. (2011). pandas: a Foundational Python Library for Data Analysis and Statistics.

674 Miglovets, M., Zagirova, S., Goncharova, N., & Mikhailov, O. (2021). Methane Emission from Palsa Mires in
675   Northeastern European Russia. *Russian Meteorology and Hydrology*, *46*(1), 52-59.
676   https://doi.org/10.3103/S1068373921010076

677 Morin, P., Porter, C., Cloutier, M., Howat, I., Noh, M.J., Willis, M., Bates, B., Willamson, C. and Peterman, K.
678   (2016). ArcticDEM; a publically available, high resolution elevation model of the Arctic. EGU General
679   Assembly 2016, Vienna, Austria.

680 Obu, J. (2021). How Much of the Earth's Surface is Underlain by Permafrost? *Journal of Geophysical Research:*
681   *Earth Surface*, *126*(5), e2021JF006123. https://doi.org/https://doi.org/10.1029/2021JF006123

682 Obu, J., Westermann, S., Kääb, A., & Bartsch, A. (2018). *Ground Temperature Map, 2000-2016, Northern*
683   *Hemisphere Permafrost* PANGAEA. https://doi.org/10.1594/PANGAEA.888600

684 Olvmo, M., Holmer, B., Thorsson, S., Reese, H., & Lindberg, F. (2020). Sub-arctic palsa degradation and the
685   role of climatic drivers in the largest coherent palsa mire complex in Sweden (Vissátvuopmi), 1955–
686   2016. *Scientific Reports*, *10*(1), 8937. https://doi.org/10.1038/s41598-020-65719-1

687 Otto, J. c., Keuschnig, M., Götz, J., Marbach, M., & Schrott, L. (2012). Detection of mountain permafrost by
688   combining high resolution surface and subsurface information–an example from the Glatzbach
689   catchment, Austrian Alps. *Geografiska Annaler: Series A, Physical Geography*, *94*(1), 43-57.
690   https://doi.org/10.1111/j.1468-0459.2012.00455.x

691 QGIS, D. (2022). QGIS User Guide: 24.2.1 Raster Analysis. Retrieved from
692   https://docs.qgis.org/3.16/en/docs/user_manual/processing_algs/gdal/rasteranalysis.html#hillshade

693 Ramage, J., Jungsberg, L., Wang, S. N., Westermann, S., Lantuit, H., & Heleniak, T. (2021). Population living
694   on permafrost in the Arctic. *Population and Environment*, *43*(1), 22-38.
695   https://doi.org/10.1007/s11111-020-00370-6

696 Reinosch, E., Buckel, J., Dong, J., Gerke, M., Baade, J., & Riedel, B. (2020). InSAR time series analysis of
697   seasonal surface displacement dynamics on the Tibetan Plateau. *The Cryosphere*, *14*(5), 1633-1650.
698   https://doi.org/10.5194/tc-14-1633-2020

699 Sannel, A. B. K. (2020). Ground temperature and snow depth variability within a subarctic peat plateau
700   landscape. *Permafrost and Periglacial Processes*, *31*(2), 255-263. https://doi.org/10.1002/ppp.2045

Sannel, A. B. K., Hugelius, G., Jansson, P., & Kuhry, P. (2016). Permafrost Warming in a Subarctic Peatland – Which Meteorological Controls are Most Important?. *Permafrost and Periglacial Processes*, 27(2), 177-188. https://doi.org/10.1002/ppp.1862

Sannel, A. B. K., & Kuhry, P. (2011). Warming-induced destabilization of peat plateau/thermokarst lake complexes. *Journal of Geophysical Research: Biogeosciences*, 116(G3). https://doi.org/10.1029/2010JG001635

Schuur, E. A. G., McGuire, A. D., Schädel, C., Grosse, G., Harden, J. W., Hayes, D. J., Hugelius, G., Koven, C. D., Kuhry, P., Lawrence, D. M., Natali, S. M., Olefeldt, D., Romanovsky, V. E., Schaefer, K., Turetsky, M. R., Treat, C. C., & Vonk, J. E. (2015). Climate change and the permafrost carbon feedback. *Nature*, 520(7546), 171-179. https://doi.org/10.1038/nature14338

Schuur, E. A. G., Vogel, J. G., Crummer, K. G., Lee, H., Sickman, J. O., & Osterkamp, T. E. (2009). The effect of permafrost thaw on old carbon release and net carbon exchange from tundra. *Nature*, 459(7246), 556-559. https://doi.org/10.1038/nature08031

Seppälä, M. (2011). Synthesis of studies of palsa formation underlining the importance of local environmental and physical characteristics. *Quaternary Research*, 75(2), 366-370. https://doi.org/10.1016/j.yqres.2010.09.007

Siewert, M.B., 2018. High-resolution digital mapping of soil organic carbon in permafrost terrain using machine learning: a case study in a sub-Arctic peatland environment. *Biogeosciences,* 15, 1663-1682.

Sjöberg, Y., Siewert, M.B., Rudy, A.C.A., Paquette, M., Bouchard, F., Malenfant-Lepage, J., Fritz, M., 2020. Hot trends and impact in permafrost science. *Permafrost and Periglacial Processes*, 31, 461-471.

Short, N., LeBlanc, A.-M., Sladen, W., Oldenborger, G., Mathon-Dufour, V., & Brisco, B. (2014). RADARSAT-2 D-InSAR for ground displacement in permafrost terrain, validation from Iqaluit Airport, Baffin Island, Canada. *Remote Sensing of Environment*, 141, 40-51. https://doi.org/https://doi.org/10.1016/j.rse.2013.10.016

SMHI, (2022). Download Meteorological observations. Retrieved from https://www.smhi.se/data/meteorologi/ladda-ner-meteorologiska-observationer#param=airtemperatureInstant,stations=core,stationid=191910

Smith, M. W., & Riseborough, D. W. (1996). Permafrost monitoring and detection of climate change. *Permafrost and Periglacial Processes*, 7(4), 301-309. https://doi.org/https://doi.org/10.1002/(SICI)1099-1530(199610)7:4<301::AID-PPP231>3.0.CO;2-R

Smith, S.L, O'Neill, H.B., Isaksen, K., Noetzli, J. and Romanovsky, V.E. (2022). The changing thermal state of permafrost. *Nature Reviews Earth and Environment,* 3, 10-23.

Sowter, A., Bin Che Amat, M., Cigna, F., Marsh, S., Athab, A., & Alshammari, L. (2016). Mexico City land subsidence in 2014–2015 with Sentinel-1 IW TOPS: Results using the Intermittent SBAS (ISBAS) technique. *International Journal of Applied Earth Observation and Geoinformation*, 52, 230-242. https://doi.org/https://doi.org/10.1016/j.jag.2016.06.015

Spyder Website Contributors. (2021). Spyder IDE. Retrieved from https://www.spyder-ide.org/

Swingedouw, D., Ifejika Speranza, C., Bartsch, A., Durand, G., Jamet, C., Beaugrand, G., & Conversi, A. (2020). Early Warning from Space for a Few Key Tipping Points in Physical, Biological, and Social-Ecological Systems. *Surveys in Geophysics*, 41(6), 1237-1284. https://doi.org/10.1007/s10712-020-09604-6

Tarnocai, C., Canadell, J. G., Schuur, E. A. G., Kuhry, P., Mazhitova, G., & Zimov, S. (2009). Soil organic carbon pools in the northern circumpolar permafrost region. *Global Biogeochemical Cycles*, 23(2). https://doi.org/https://doi.org/10.1029/2008GB003327

Torres, R., Snoeij, P., Geudtner, D., Bibby, D., Davidson, M., Attema, E., Potin, P., Rommen, B., Floury, N., Brown, M., Traver, I. N., Deghaye, P., Duesmann, B., Rosich, B., Miranda, N., Bruno, C., L'Abbate, M., Croci, R., Pietropaolo, A., . . . Rostan, F. (2012). GMES Sentinel-1 mission. *Remote Sensing of Environment*, 120, 9-24. https://doi.org/https://doi.org/10.1016/j.rse.2011.05.028

Turetsky, M. R., Abbott, B. W., Jones, M. C., Anthony, K. W., Olefeldt, D., Schuur, E. A. G., Grosse, G., Kuhry, P., Hugelius, G., Koven, C., Lawrence, D. M., Gibson, C., Sannel, A. B. K., & McGuire, A. D. (2020). Carbon release through abrupt permafrost thaw. *Nature Geoscience*, 13(2), 138-143. https://doi.org/10.1038/s41561-019-0526-0

Vallée, S., & Payette, S. (2007). Collapse of permafrost mounds along a subarctic river over the last 100 years (northern Québec). *Geomorphology*, 90, 162-170. https://doi.org/10.1016/j.geomorph.2007.01.019

van Huissteden, J., Teshebaeva, K., Cheung, Y., Magnússon, R. Í., Noorbergen, H., Karsanaev, S. V., Maximov, T. C., & Dolman, A. J. (2021). Geomorphology and InSAR-Tracked Surface Displacements in an Ice-Rich Yedoma Landscape. *Frontiers in Earth Science*, 9(724). https://doi.org/10.3389/feart.2021.680565

Varner, R. K., Crill, P. M., Frolking, S., McCalley, C. K., Burke, S. A., Chanton, J. P., Holmes, M. E., null, n., Saleska, S., & Palace, M. W. (2022). Permafrost thaw driven changes in hydrology and vegetation

cover increase trace gas emissions and climate forcing in Stordalen Mire from 1970 to 2014. *Philosophical Transactions of the Royal Society A: Mathematical, Physical and Engineering Sciences*, *380*(2215), 20210022. https://doi.org/10.1098/rsta.2021.0022

Vikhamar-Schuler, D., Isaksen, K., Haugen, J. E., Tømmervik, H., Luks, B., Schuler, T. V., & Bjerke, J. W. (2016). Changes in Winter Warming Events in the Nordic Arctic Region. *Journal of Climate*, *29*(17), 6223-6244. https://doi.org/10.1175/JCLI-D-15-0763.1

Virtanen, P., Gommers, R., Oliphant, T. E., Haberland, M., Reddy, T., Cournapeau, D., Burovski, E., Peterson, P., Weckesser, W., & Bright, J. (2020). SciPy 1.0: fundamental algorithms for scientific computing in Python. *Nature methods*, *17*(3), 261-272.

Vorren, K.-D. (2017). The first permafrost cycle in Færdesmyra, eastern Finnmark, Norway? *Norsk Geografisk Tidsskrift - Norwegian Journal of Geography*, *71*(2), 114-121. https://doi.org/10.1080/00291951.2017.1316309

Zuidhoff, F. S. (2002). Recent decay of a single palsa in relation to weather conditions between 1996 and 2000 in Laivadalen, northern Sweden. *Geografiska Annaler Series A-Physical Geography*, *84A*(2), 103-111. https://doi.org/10.1111/j.0435-3676.2002.00164.x

Zuidhoff, F. S., & Kolstrup, E. (2000). Changes in palsa distribution in relation to climate change in Laivadalen, northern Sweden, especially 1960–1997. *Permafrost and Periglacial Processes*, *11*(1), 55-69. https://doi.org/https://doi.org/10.1002/(SICI)1099-1530(200001/03)11:1